Inorganic Chemistry

Article

pubs.acs.org/IC

Dual Emissions from Ruthenium(II) Complexes Having 4-Arylethynyl-1,10-phenanthroline at Low Temperature

Eri Sakuda,*[,†,‡,§,⊥] Chiaki Matsumoto,[†] Yuki Ando,[†] Akitaka Ito,[†,∥] Kousuke Mochida,[†] Atsushi Nakagawa,[‡] and Noboru Kitamura*[,†,‡]

[†]Department of Chemistry, Faculty of Science, [‡]Department of Chemical Sciences and Engineering, Graduate School of Chemical Sciences and Engineering, Hokkaido University, Sapporo 060-0810, Japan

[§]PRESTO, Japan Science and Technology Agency, Honcho, Kawaguchi, Saitama Prefecture 332-0012, Japan

[∥]Department of Chemistry, Graduate School of Science, Osaka City University, Osaka 558-8585, Japan

ABSTRACT: A $[Ru(phen)_3]^{2+}$ complex (phen = 1,10-phenanthroline) having an arylethynyl group at the 4-position of one of the three phen ligands (aryl: (dimesityl)borylduryl group = $[\mathbf{RuBE}]^{2+}$ or duryl group = $[\mathbf{RuDE}]^{2+}$) showed dual emissions at low temperature in propylene carbonate (PC). The shorter emission lifetime components ($\tau^{em}(s) \approx 13$ μs) that originated from the lowest-energy excited triplet states (T_1) of the complexes were almost independent of temperature (T = 77−320 K), while the longer emission lifetime components ($\tau^{em}(l)$), as the T_2 emissions appeared below the fluid-to-glass transition temperature ($T_g \approx 220$ K) in PC, were almost constant at 27 μs in the range of T = 77−220 K. The $\tau^{em}(s)$ components of the complexes were assigned to the emissions from the metal-to-ligand charge transfer (MLCT) excited states possessing relatively large ligand-centered (LC) excited-state characters (T_1(MLCT/LC)), while the $\tau^{em}(l)$ components were shown to be originating from the T_2(MLCT) excited states. The T_2(MLCT) states of the complexes became nonemissive above T_g in PC due to fast nonradiative decay through solvent reorganization around the T_2(MLCT) excited states. The photophysical properties of the complexes were also shown to be characterized by the presence of the arylethynyl units at the 4-positions of the phen ligands.

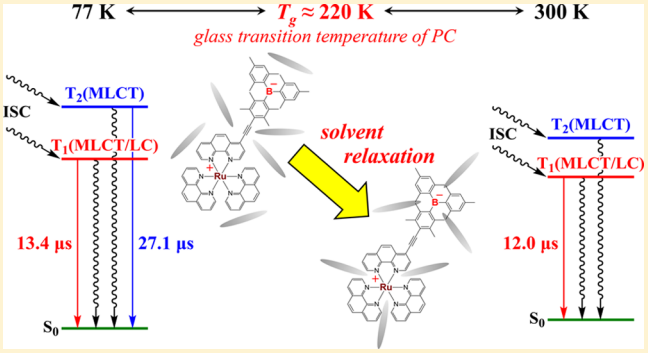

INTRODUCTION

We reported recently that $[Ru(phen)_2\{4\text{-(dimesityl)-boryldurylethynyl-phen}\}]^{2+}$ ($[\mathbf{RuBE}]^{2+}$, phen = 1,10-phenanthroline, see Chart 1 for the structure) showed long-lived metal-to-ligand charge transfer (MLCT) emission in CH_3CN at 298 K with the quantum yield (Φ^{em}) and lifetime (τ^{em}) being 0.11 and 12 μs, respectively.[1] Commonly, the emission lifetime of a polypyridyl Ru(II) complex at room temperature decreases upon temperature (T) elevation, owing to thermal activation from the emitting MLCT excited triplet state (^{3}MLCT*) to the nonemitting dd* excited triplet state (^{3}dd*) and subsequent fast nonradiative decay from ^{3}dd* to the ground state.[1,2] Nonetheless, the emission lifetime of $[\mathbf{RuBE}]^{2+}$ is almost independent of T at τ^{em} = 10.7 (280 K)−9.8 μs (330 K) in propylene carbonate[1] and, thus, the long-lived and T-independent emission from $[\mathbf{RuBE}]^{2+}$ is extraordinary among those of various polypyridyl Ru(II) complexes hitherto reported.[2] The unique photophysical properties of $[\mathbf{RuBE}]^{2+}$ could be explained by the participation of the CT interaction between the π-orbital of the aryl group (π(aryl)) and the vacant p-orbital on the boron atom (p(B), π(aryl)-p(B) CT) in the 4-(dimesityl)boryldurylethynyl-phen (DBDE-phen) ligand. The synergistic MLCT/π(aryl)-p(B) CT interactions result in stabilization of the ^{3}MLCT* energy relative to the ^{3}dd* energy, and this brings about inhibition of thermal activation from ^{3}MLCT* to ^{3}dd*, giving rise to long-lived and T-independent emission of $[\mathbf{RuBE}]^{2+}$.[1] Particular MLCT/π(aryl)-p(B) CT interactions similar to those of $[\mathbf{RuBE}]^{2+}$ have been

Chart 1. Structures of $[\mathbf{RuBE}]^{2+}$ and $[\mathbf{RuDE}]^{2+}$

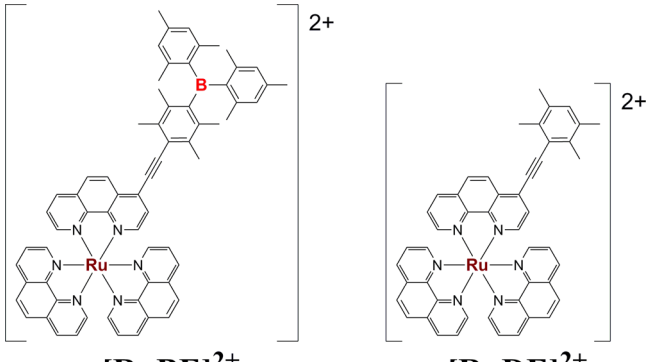

$[\mathbf{RuBE}]^{2+}$ $[\mathbf{RuDE}]^{2+}$

Received: December 1, 2014
Published: March 6, 2015

DOI: 10.1021/ic502843x
Inorg. Chem. 2015, 54, 3245−3252

observed for Pt(II), Re(I), and Ir(III) complexes bearing triarylborane-appended ligands, and these complexes also exhibit relatively intense and/or long-lived emission in solution at room temperature compared with the relevant complex without a triarylborane group.[3]

It is worth pointing out that a transition metal complex having a 4- or 4,7-substituted phen ligand sometimes shows unusual emission behaviors. As an example, Wallace et al. reported that $[Re(CO)_3(4,7\text{-disubstituted-phen})(pyridine)]^+$ showed both MLCT and ligand-centered (LC) emissions at low temperature.[4] As an analogous complex to $[\mathbf{RuBE}]^{2+}$, furthermore, Glazer et al. reported $[Ru(bpy)_2\{4\text{-}(4'\text{-R-phenylethynyl})phen\}]^{2+}$ (bpy = 2,2′-bipyridine; R = −H, $-OCH_3$, or $-CF_3$) exhibited dual emissions in CH_3CN at room temperature. Typically, the long ($\tau^{em}(l)$) and short lifetime components ($\tau^{em}(s)$) of the complex with R = −H, $-OCH_3$, or $-CF_3$ is reported to be 6.6 and 1.2, 11.5 and 1.1, or 6.6 and 1.3 μs, respectively, and the authors have attributed the $\tau^{em}(l)$ and $\tau^{em}(s)$ components to the Ru(II)-to-π*(phen) and Ru(II)-to-π*(bpy) MLCT emissions, respectively.[5] The results by Glazer et al. suggest that the Ru(II) complex having a 4- or 4,7-arylethynyl-phen ligand in general shows long-lived emission similar to $[\mathbf{RuBE}]^{2+}$. Therefore, the role of the arylborane CT unit of $[\mathbf{RuBE}]^{2+}$ in the long-lived emission is worth studying in more detail. Furthermore, although $[\mathbf{RuBE}]^{2+}$ displays single emission in solution at or near room temperature (T = 280−330 K),[1] the complex might exhibit dual emissions at low temperature similar to the case of $[Re(CO)_3(4,7\text{-disubstituted-phen})(pyridine)]^+$.

In this paper, we report the emission characteristics of $[\mathbf{RuBE}]^{2+}$ and $[Ru(phen)_2\{4\text{-durylethynyl-phen}\}]^{2+}$ ($[\mathbf{RuDE}]^{2+}$, see Chart 1) in propylene carbonate in the T range of 77−330 K and demonstrate that both $[\mathbf{RuBE}]^{2+}$ and $[\mathbf{RuDE}]^{2+}$ exhibit dual emissions below 220 K as confirmed by time-resolved emission spectroscopy. The origin of the dual emissions from the complexes is then discussed on the basis of the results of Franck−Condon emission spectral fitting analysis and time-dependent density functional theory (TD-DFT) calculations.

EXPERIMENTAL SECTION

The PF_6 salts of $[\mathbf{RuBE}]^{2+}$ and $[\mathbf{Ru(phen)_3}]^{2+}$ used in the present experiments were essentially the same with those reported earlier.[1] All of the chemicals used for the synthesis of $[\mathbf{RuDE}]^{2+}$ were supplied from Wako Pure Chemicals Industries, Ltd., Kanto Chemicals Co., Inc., Tokyo Chemical Industry Co., Ltd., or Sigma−Aldrich Co., LLC. Column chromatography was carried out by using GE Healthcare Sephadex LH-20.

^{1}H NMR spectra were recorded on a JEOL JME-EX270 FT-NMR system (270 MHz). The chemical shifts of the spectra determined in $CDCl_3$ or CD_3CN were given in ppm, with tetramethylsilane being an internal standard (0.00 pm).

Synthesis of $[Ru(phen)_2\{4\text{-durylethynyl-phen}\}]^{2+}$ PF_6 salt: $[\mathbf{RuDE}](PF_6)_2$. After an oven-dried Schlenk tube was evacuated and filled with an Ar gas, $[Ru(phen)_2(4\text{-Br-phen})](PF_6)_2$ (128 mg, 0.101 mmol),[1] CuI (2.1 mg, 0.011 mmol), and [1,1′-bis(diphenylphosphino)ferrocene]dichloropalladium(II) ($[Pd(dppf)Cl_2]\cdot CH_2Cl_2$, 8.0 mg, 0.0098 mmol) were added, and the tube was evacuated and filled with Ar gas. An argon gas-purged *N*,*N*-dimethylformamide (DMF, 5 mL)/triethylamine (2 mL) mixture was added to the tube. A DMF (10 mL)/triethylamine (4 mL) solution of ethynyldurene (158 mg, 0.998 mmol)[6] was then added to the reaction mixture, which was stirred at room temperature for 1 h under N_2 gas atmosphere. Insoluble solids were removed by filtration through Celite, and the filtrate was added dropwise to a sufficient amount of an acetone/*n*-hexane mixture, giving red precipitates. The crude product was purified successively by column chromatography (LH-20, ethanol/CH_3CN = 1/1, v/v) and recrystallization from an ethanol/CH_3CN mixture, affording the PF_6 salt of $[\mathbf{RuDE}]^{2+}$ as red solids (53.8 mg, 49%). ^{1}H NMR (270 MHz, CD_3CN): δ 2.24 (s, 6H, CH_3 *ortho* of duryl), 2.51 (s, 6H, CH_3 *meta* of duryl), 7.08 (s, 1H, Ar−H of duryl), 7.57−7.64 (m, 5H, 3,8-Ar-H of phen, 8-Ar-H of 4-DE-phen), 7.70 (d, 1H, J = 5.6 Hz, 6-Ar-H of 4-DE-phen), 7.96−8.04 (m, 5H, 4,7-Ar-H of phen, 5-Ar-H of 4-DE-phen), 8.09 (dd, 1H, J = 1.2, 5.3 Hz, 7-Ar-H of 4-DE-phen), 8.23 (s, 4H, 5,6-Ar-H of phen), 8.33 (d, 1H, J = 9.0 Hz, 3-Ar-H of 4-DE-phen), 8.56−8.62 (m, 6H, 2,9-Ar of phen, 2,9-Ar-H of 4-DE-phen).

Spectroscopic Measurements. Acetonitrile and propylene carbonate as the solvents for spectroscopic and photophysical measurements were distilled prior to use by the accepted procedures.[7] Absorption and corrected emission spectra of the complexes were measured by a Hitachi UV-3300 or Hitachi U-3900H spectrophotometer and a red-sensitive multichannel photodetector (PMA-11, Hamamatsu Photonics, excitation wavelength = 355 nm), respectively. The absolute emission quantum yields of the complexes were measured by a Hamamatsu C9920−02 system equipped with an integrating sphere and a red-sensitive multichannel photodetector (PMA-12) at 450 nm excitation. The absorbance of a sample solution was set <0.05 at the excitation wavelength. Emission lifetime and time-resolved emission spectroscopy (corrected) measurements were conducted by using a streak camera (Hamamatsu Photonics, C4334) as a photodetector by 355- or 532-nm pulse laser excitation (LOTIS TII Ltd.). A liquid N_2 cryostat (Oxford Instruments, DN1704 optical Dewar and 3120 temperature controller) was used to control a sample temperature. For emission spectroscopy, sample solutions were deaerated by purging an Ar gas stream over 30 min and sealed at the constriction of an optical quartz cell.

Theoretical Calculations. Theoretical calculations for the complexes were conducted with the Gaussian 09W software.[8] Optimization of the ground-state structures of the complexes were performed by using DFT with the B3LYP function. The LanL2DZ and 6-31G(d,p) basis sets were used to treat the geometrical structures of ruthenium and all other atoms, respectively. TD-DFT calculations were then performed to estimate the energies and oscillator strengths of the lowest-energy singlet transitions. Although the results of the TD-DFT calculations on $[\mathbf{RuBE}]^{2+}$ were already reported in a previous publication,[1] the calculations using these basis sets gave better fits to the experimental results than the previous ones. Therefore, the present report also includes the TD-DFT calculations on $[\mathbf{RuBE}]^{2+}$. The calculations on both $[\mathbf{RuBE}]^{2+}$ and $[\mathbf{RuDE}]^{2+}$ were performed in acetonitrile as a solvent by using a Polarizable Continuum Model (PCM). Kohn−Sham orbitals were plotted using GaussView 5.0.[9]

RESULTS AND DISCUSSION

Absorption and Emission Characteristics at 298 K. Figure 1 shows the absorption (upper) and emission (lower) spectra of $[\mathbf{RuBE}]^{2+}$ and $[\mathbf{RuDE}]^{2+}$ in CH_3CN at 298 K together with those of $[\mathbf{Ru(phen)_3}]^{2+}$ as a reference, and the spectroscopic data (absorption maximum wavelength (λ^{abs}), molar absorption coefficient (ε), and the emission maximum wavelength (λ^{em})) are summarized in Table 1.

The MLCT absorption maximum of $[\mathbf{RuBE}]^{2+}$ or $[\mathbf{RuDE}]^{2+}$ was shifted to the longer wavelength compared with that of $[\mathbf{Ru(phen)_3}]^{2+}$ owing to the presence of the arylethynyl group in the phen ligand. Furthermore, both $[\mathbf{RuBE}]^{2+}$ and $[\mathbf{RuDE}]^{2+}$ exhibited absorption bands at ∼376 nm. Since $[\mathbf{Ru(phen)_3}]^{2+}$ shows no absorption peak in this wavelength region, the bands observed for $[\mathbf{RuBE}]^{2+}$ and $[\mathbf{RuDE}]^{2+}$ could be assigned to the ππ* (LC) transitions of the durylethynyl groups in the DBDE- and DE-phen ligands, respectively. It is worth emphasizing that the absorption band intensities of $[\mathbf{RuBE}]^{2+}$ in 300−550 nm decrease considerably in the presence of tetra-*n*-butylammo-

DOI: 10.1021/ic502843x
Inorg. Chem. 2015, 54, 3245−3252

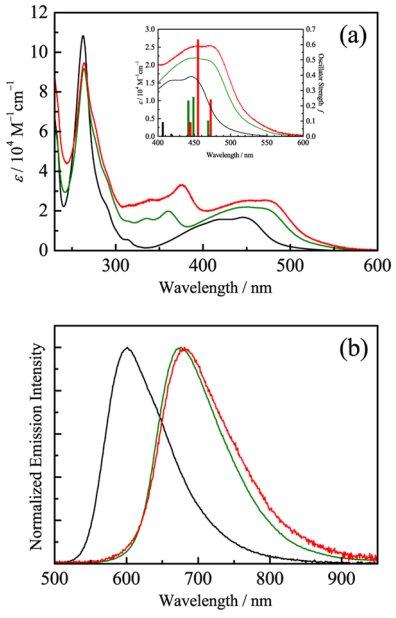

Figure 1. Absorption (a) and corrected emission (b) spectra of $[\mathbf{RuBE}]^{2+}$ (red), $[\mathbf{RuDE}]^{2+}$ (green), and $[\mathbf{Ru(phen)_3}]^{2+}$ (black) in CH_3CN at 298 K. (inset) The comparisons between the experimentally-observed absorption spectra and oscillator strengths of the lowest-energy absorption transitions of the complexes predicted by the TD-DFT calculations. The absorption and emission spectra of $[\mathbf{RuBE}]^{2+}$ and $[\mathbf{Ru(phen)_3}]^{2+}$ were taken from ref 1.

nium fluoride (TBAF) through coordination of F^- with p(B).[1] Therefore, the π(aryl)-p(B) CT interaction in the DBDE-phen ligand also participates to the MLCT absorption transitions in $[\mathbf{RuBE}]^{2+}$ as reported previously.[1]

To discuss further the spectroscopic properties, we conducted TD-DFT calculations on the molecular-orbital (MO) distributions in the highest-energy occupied MO (HOMO) and lowest-energy unoccupied MO (LUMO) levels of $[\mathbf{RuBE}]^{2+}$ and $[\mathbf{RuDE}]^{2+}$ as the data are shown in Figure 2. We also calculated the oscillator strengths of the lowest-energy absorption transitions of the complexes. The results are shown in Figure 1a as an inset, together with the experimentally-observed absorption spectra of the complexes. The calculations were in good agreement with the experimentally-observed absorption spectra of the complexes. The results of the TD-DFT calculations demonstrated that the lowest-energy absorption transitions in $[\mathbf{RuBE}]^{2+}$ and $[\mathbf{RuDE}]^{2+}$ were ascribed to the degenerated HOMO−1(59%)/HOMO(41%) → LUMO(85%)/LUMO+3(15%) and degenerated HOMO−1(54%)/HOMO(46%) → LUMO(78%)/LUMO+3(22%) transitions, respectively, with minor contributions of HOMO−1/HOMO → LUMO+1/LUMO+2 absorption transitions for both complexes. As seen in Figure 2, the HOMO−1 levels in $[\mathbf{RuBE}]^{2+}$ and $[\mathbf{RuDE}]^{2+}$ are characterized by the electron densities on the Ru(II) atoms and those partly on the pyridine rings in the arylethynyl-phen/phen ligands, while the electrons in the HOMO levels are distributed to both Ru(II) atoms and arylethynyl moieties. On the other hand, the MOs in the LUMO levels of $[\mathbf{RuBE}]^{2+}$ and $[\mathbf{RuDE}]^{2+}$ distribute to the entire arylethynyl-phen ligand. In the case of $[\mathbf{RuBE}]^{2+}$, furthermore, the MO in the LUMO level is also distributed to the p-orbital on the boron atom, while that in the LUMO+3 level extends to the pyridine ring in the arylethynyl-phen lignd and the durylethynyl unit. The MO in the LUMO+3 level of $[\mathbf{RuDE}]^{2+}$ resides primarily on the phen ring of the arylethynyl-phen ligand. These data suggest that the lowest-energy absorption transitions in $[\mathbf{RuBE}]^{2+}$ and $[\mathbf{RuDE}]^{2+}$ are responsible for the MLCT-type transitions with relatively large (HOMO → LUMO) and small LC characters (HOMO−1 → LUMO/LUMO+3), respectively, while the MLCT-type HOMO → LUMO+3 transition also contributes slightly to the lowest-energy absorption in $[\mathbf{RuDE}]^{2+}$. Furthermore, π(aryl)-p(B) CT also contributes to the lowest-energy MLCT/LC absorption in $[\mathbf{RuBE}]^{2+}$, which agrees very well with the TBAF effects on the absorption spectrum of $[\mathbf{RuBE}]^{2+}$ as described above and a previous publication.[1] It is worth noting that, since the MO in the LUMO of $[\mathbf{RuBE}]^{2+}$ extends partly to p(B), it is predicted that the transition dipole moment in the lowest-energy absorption of $[\mathbf{RuBE}]^{2+}$ should be larger than that of $[\mathbf{RuDE}]^{2+}$. In practice, this is shown experimentally by the larger ε value of the MLCT/LC absorption band of $[\mathbf{RuBE}]^{2+}$ relative to that of $[\mathbf{RuDE}]^{2+}$.

$[\mathbf{RuDE}]^{2+}$ also showed intense and long-lived emission at 675 nm similar to $[\mathbf{RuBE}]^{2+}$ with Φ^{em} and τ^{em} being 0.11 and 13 μs, respectively, as the data were included in Table 1. The Φ^{em} and τ^{em} values of $[\mathbf{RuBE}]^{2+}$ and $[\mathbf{RuDE}]^{2+}$ are very much higher and longer, respectively, than the relevant value of $[\mathbf{Ru(phen)_3}]^{2+}$. Although the π(aryl)-p(B) CT interaction participates in the emissive excited state of $[\mathbf{RuBE}]^{2+}$ as revealed by emission quenching by TBAF as reported previously,[1] the intense and long-lived emission from $[\mathbf{RuDE}]^{2+}$ demonstrates that the presence of the dimesitylboryl group in $[\mathbf{RuBE}]^{2+}$ is not the main factor governing the emission characteristics of the complex, but the durylethynyl unit at the 4-position of phen plays an important role in the intense and long-lived emission from $[\mathbf{RuBE}]^{2+}$ and $[\mathbf{RuDE}]^{2+}$. The radiative (k_r) and nonradiative decay rate constants (k_{nr}) evaluated by the relations $\Phi^{em} = k_r/(k_r + k_{nr})$ and $\tau^{em} = (k_r + k_{nr})^{-1}$ were almost the same between $[\mathbf{RuBE}]^{2+}$ and $[\mathbf{RuDE}]^{2+}$, and were smaller by factors of ∼10 and ∼20, respectively, than the relevant value of $[\mathbf{Ru(phen)_3}]^{2+}$ (see Table 1). The present data demonstrate that the excited-state characteristics of $[\mathbf{Ru(phen)_3}]^{2+}$ can be modulated considerably by an introduction of the durylethynyl unit at the 4-position of a phen ligand. Furthermore, since the lowest-energy absorption transition in $[\mathbf{RuBE}]^{2+}$ or $[\mathbf{RuDE}]^{2+}$ involves partly the $\pi\pi^*$ (LC) transition localized primarily in the durylethynyl-phen

Table 1. Spectroscopic and Photophysical Parameters of the Complexes in CH_3CN at 298 K

complex	λ^{abs}, nm (ε, 10^4 $M^{-1}cm^{-1}$)			λ^{em}, nm	τ^{em}, μs	Φ^{em}	k_r	k_{nr}
							10^4 s^{-1}	
$[\mathbf{RuBE}]^{2+}$ [a]	265 (9.5)	376 (3.3)	473 (2.6)	681	12	0.11	0.92	7.4
$[\mathbf{RuDE}]^{2+}$	263 (9.1)	360 (2.0)	471 (2.1)	675	13	0.11	0.85	6.8
$[\mathbf{Ru(phen)_3}]^{2+}$ [a]	263 (11)		445 (1.7)	599	0.42	0.045	11	230

[a]Data compiled from ref 1.

DOI: 10.1021/ic502843x
Inorg. Chem. 2015, 54, 3245−3252

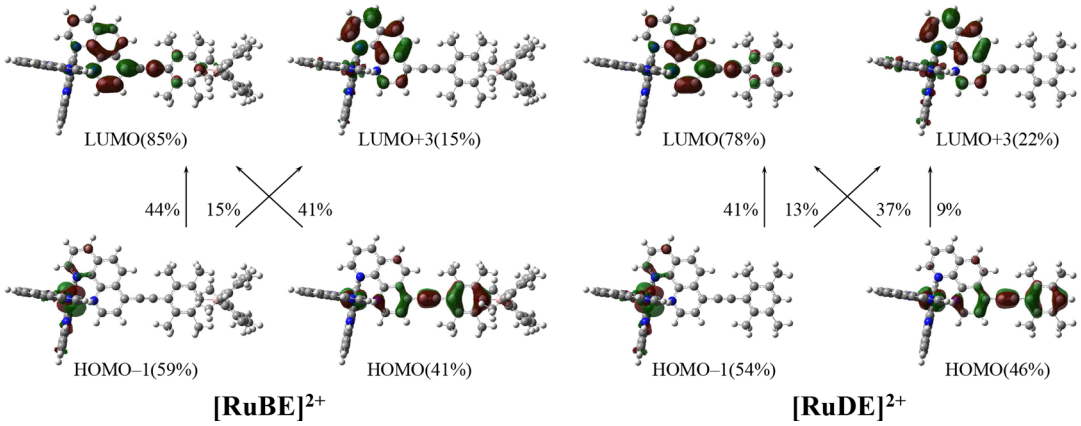

Figure 2. Molecular-orbital contours (0.03 eÅ^{-3}) of [**RuBE**]$^{2+}$ (left) and [**RuDE**]$^{2+}$ (right) in the HOMO−1, HOMO, LUMO, and LUMO+3 levels.

ligand as suggested by the TD-DFT calculations (Figure 2), the emissive excited triplet states of the complexes are also predicted to possess $\pi\pi^*$ characters. We suppose that one possible origin of the long-lived emissions from [**RuBE**]$^{2+}$ and [**RuDE**]$^{2+}$ will be the $\pi\pi^*$ characters in the emissive MLCT excited triplet states of the complexes.

Dual Emissions from [RuBE]$^{2+}$ and [RuDE]$^{2+}$ at Low Temperature. Figures 3 and 4 show the *T*-dependence of the

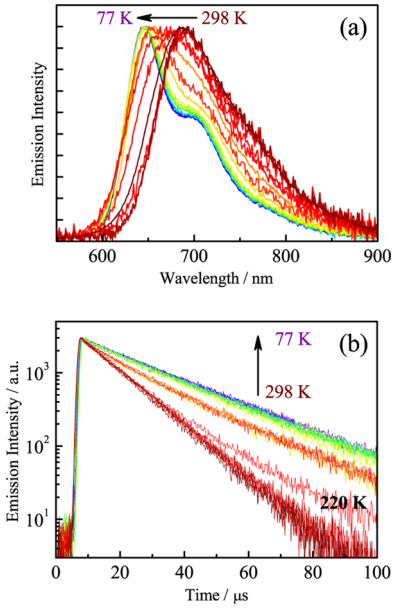

Figure 3. Temperature dependence of the emission spectrum (a) and decay profile (b) of [**RuBE**]$^{2+}$ in propylene carbonate.

emission spectra (upper) and decay profiles (lower) of [**RuBE**]$^{2+}$ and [**RuDE**]$^{2+}$ in propylene carbonate (PC), respectively. When the samples were cooled from 298 to 77 K, as seen in Figure 3a, the emission spectrum of [**RuBE**]$^{2+}$ shifted to a shorter wavelength accompanied by sharpening of the spectral band shape. Such *T*-dependent emission characteristics are commonly observed for polypyridyl Ru(II) complexes.[10] In the *T* range of 230−298 K, the emission decay profile of the complex was fitted by a single exponential function irrespective of *T* with the decay time constant at 11−13 μs whose values were almost comparable to that at 298 K, while that below 220 K obeyed with a double exponential

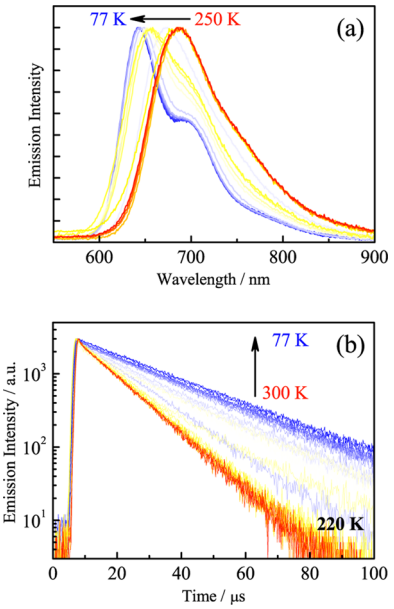

Figure 4. Temperature dependence of the emission spectrum (a) and decay profile (b) of [**RuDE**]$^{2+}$ in propylene carbonate.

function. At 220 K, the long emission lifetime component ($\tau^{em}(l) \approx 22$ μs) appeared in addition to the short emission lifetime component ($\tau^{em}(s) = 11-13$ μs): shown by 220 K in Figure 3b. At 77 K, the emission decay profile of [**RuBE**]$^{2+}$ was best fitted by $\tau^{em}(s) = 13.4$ and $\tau^{em}(l) = 27.1$ μs. The *T*-dependent emission behaviors analogous to those of [**RuBE**]$^{2+}$ were also observed for [**RuDE**]$^{2+}$ as shown in Figure 4. In practice, the emission from [**RuDE**]$^{2+}$ showed single exponential decay irrespective of *T* in 230−330 K with the time constant at ∼13 μs, while that at 77 K was best characterized by $\tau^{em}(s) = 14.1$ and $\tau^{em}(l) = 27.1$ μs.

To obtain further information on the double exponential emission decay profiles of [**RuBE**]$^{2+}$ and [**RuDE**]$^{2+}$ below 220 K, we conducted time-resolved emission spectroscopy at 77 K, and the results are shown in Figures 5a and 6a, respectively. The data clearly demonstrate that the emission spectrum of the complex shifts to a shorter wavelength with a delay time after laser excitation (*t*), indicating the $\tau^{em}(l)$ component (27.1 μs for both complexes) emits in the shorter wavelength region compared with the $\tau^{em}(s)$ component: 13.4 or 14.1 μs for [**RuBE**]$^{2+}$ or [**RuDE**]$^{2+}$, respectively. We also evaluated the

DOI: 10.1021/ic502843x
Inorg. Chem. 2015, 54, 3245−3252

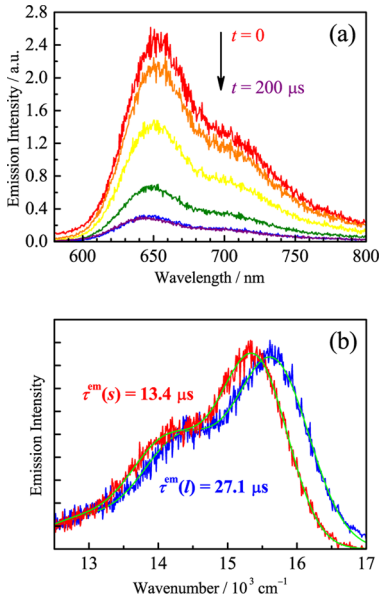

Figure 5. Time-resolved emission spectra (a) and the separated emission spectra of the $\tau^{em}(s)$ (red) and $\tau^{em}(l)$ (blue) components of $[\mathbf{RuBE}]^{2+}$ in propylene carbonate at 77 K (b). The green curves in the lower panel represent the simulated emission spectra by Franck–Condon emission spectral fittings. See the main text in detail.

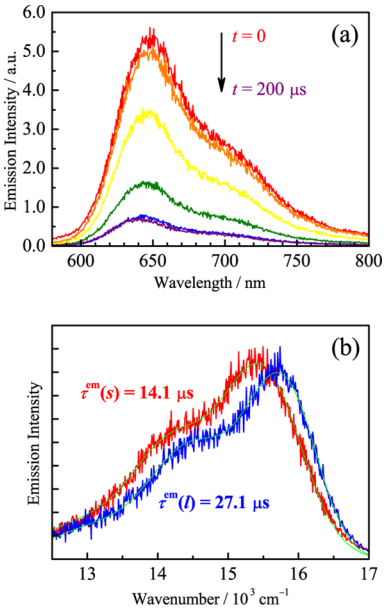

Figure 6. Time-resolved emission spectra (a) and the separated emission spectra of the $\tau^{em}(s)$ (red) and $\tau^{em}(l)$ (blue) components of $[\mathbf{RuDE}]^{2+}$ in propylene carbonate at 77 K (b). The green curves in the lower panel represent the simulated emission spectra by Franck–Condon emission spectral fittings. See the main text in detail.

emission spectra of the $\tau^{em}(s)$ and $\tau^{em}(l)$ components by subtracting the spectrum observed at $t = 0$ (gated time = 20 μs) from that at $t = 100$ μs (gated time = 100 μs). The separated emission spectra of the $\tau^{em}(s)$ and $\tau^{em}(l)$ components of $[\mathbf{RuBE}]^{2+}$ and $[\mathbf{RuDE}]^{2+}$ in a wavenumber scale are shown in Figures 5b and 6b, respectively. The emission spectral band shapes of the $\tau^{em}(s)$ and $\tau^{em}(l)$ components observed for the two complexes were very similar to each other, while the emission maximum energy ($\tilde{\nu}^{em}$) of the $\tau^{em}(l)$ component observed for $[\mathbf{RuBE}]^{2+}$ or $[\mathbf{RuDE}]^{2+}$ was higher than that of $\tau^{em}(s)$ by 270 or 290 cm^{-1}, respectively: $\tilde{\nu}^{em}(l)$ = 15 610 and $\tilde{\nu}^{em}(s)$ = 15 340 cm^{-1} for $[\mathbf{RuBE}]^{2+}$, $\tilde{\nu}^{em}(l)$ = 15 700 and $\tilde{\nu}^{em}(s)$ = 15 410 cm^{-1} for $[\mathbf{RuDE}]^{2+}$. These data demonstrate explicitly dual emissions from $[\mathbf{RuBE}]^{2+}$ and $[\mathbf{RuDE}]^{2+}$ at 77 K.

Figures 7 and 8 show the T dependence of the emission lifetimes (upper) and their percentages in each total emission

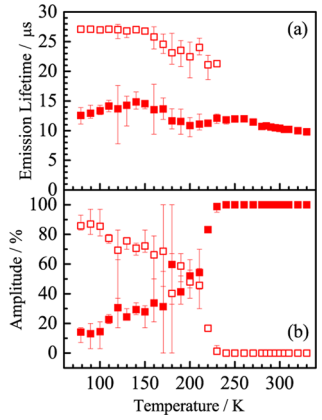

Figure 7. Temperature dependence of the emission lifetimes (a) and amplitudes (b) of the $\tau^{em}(s)$ (closed red boxes) and $\tau^{em}(l)$ components (open red boxes) of $[\mathbf{RuBE}]^{2+}$.

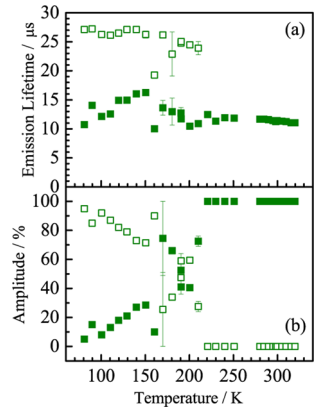

Figure 8. Temperature dependence of the emission lifetimes (a) and amplitudes (b) of the $\tau^{em}(s)$ (closed green boxes) and $\tau^{em}(l)$ components (open green boxes) of $[\mathbf{RuDE}]^{2+}$.

decay profile (lower) determined for $[\mathbf{RuBE}]^{2+}$ and $[\mathbf{RuDE}]^{2+}$, respectively. The two complexes showed analogous T-dependent emission behaviors, showing single and dual emissions above and below ~220 K, respectively. Although the data on $\tau^{em}(s)$ are somewhat scattered, both $\tau^{em}(s)$ and $\tau^{em}(l)$ values of the complexes have been evaluated to increase with a decrease in T from 220 to 150 K, while the values below 150 K reach almost constant at $\tau^{em}(s) \approx 13$ μs and $\tau^{em}(l) \approx 27$ μs. For a least-mean squares analysis of double-exponential emission decay, short and long lifetime components are likely to be simulated to be longer and shorter, respectively, compared with their actual emission lifetimes, in particular, when the two decay time constants and their percentages in a total emission decay profile (i.e., amplitude) are close with one another. In the T range of 150–220 K, therefore, we suppose that the actual $\tau^{em}(s)$ and $\tau^{em}(l)$ values of both $[\mathbf{RuBE}]^{2+}$ and $[\mathbf{RuDE}]^{2+}$ would be almost constant at ~13 and ~27 μs, respectively, as observed at 77 K. It is worth emphasizing that, although the

DOI: 10.1021/ic502843x
Inorg. Chem. 2015, 54, 3245–3252

Table 2. Franck−Condon Fitting Parameters

complex	component	E_0, cm^{-1}	$\Delta\tilde{\nu}_{1/2}$, cm^{-1}	$\hbar\omega_M$, cm^{-1}	S_M	$\hbar\omega_L$, cm^{-1}	S_L
$[\mathbf{RuBE}]^{2+}$	$\tau^{em}(s)$	15 580	980	1330	0.71	380	0.88
	$\tau^{em}(l)$	15 740	1180	1380	0.78	430	0.36
$[\mathbf{RuDE}]^{2+}$	$\tau^{em}(s)$	15 620	1210	1350	0.79	400	0.56
	$\tau^{em}(l)$	15 990	940	1400	0.73	430	1.03
$[\mathbf{Ru(phen)_3}]^{2+}$		17 660	730	1410	0.89	420	1.04

$\tau^{em}(l)$ component of $[\mathbf{RuBE}]^{2+}$ or $[\mathbf{RuDE}]^{2+}$ emits in a higher energy by 270 or 290 cm^{-1}, respectively, compared with the relevant $\tau^{em}(s)$ component (at 77 K) as described before, the contribution of $\tau^{em}(l)$ to each total decay profile increases with a decrease in T below 220 K, in particular, even below 150 K as seen in Figures 7b and 8b. This demonstrates explicitly that thermal interconversion between the excited states responsible for $\tau^{em}(s)$ and $\tau^{em}(l)$ does not take place in the present system. Therefore, we conclude that two isolated excited triplet states show individual emissions below 220 K. In practice, the thermal energy (i.e., k_BT, where k_B is the Boltzmann constant) does not exceed the energy gap between the two excited states irrespective of T: 270−290 cm^{-1} > k_BT = 50 (77 K)−220 cm^{-1} (320 K).

Franck−Condon Emission Spectral Fitting Analysis. We conducted Franck−Condon emission spectral fitting analysis of the complexes based on eq 1.[11] In eq 1, $I(\tilde{\nu})$ is the emission intensity at an energy $\tilde{\nu}$ in wavenumber relative to that of the 0−0 emission transition. E_0 is the energy gap between the zeroth vibrational levels in the ground and emitting excited states. $\hbar\omega_M$ and $\hbar\omega_L$ are the medium- and low-frequency accepting vibration modes inducing nonradiative decay, respectively, and S_M or S_L is the relevant Huang−Rhys factor for the emission transition. $\Delta\tilde{\nu}_{1/2}$ is the full-width at half-maximum of an individual emission vibronic line. Summation in eq 1 was made for 11 vibrational levels (v_M or v_L: 0 → 10). The emission spectra of the $\tau^{em}(s)$ and $\tau^{em}(l)$ components observed for $[\mathbf{RuBE}]^{2+}$ and $[\mathbf{RuDE}]^{2+}$ at 77 K shown in Figures 5b and 6b, respectively, were then simulated by eq 1 with E_0, $\Delta\tilde{\nu}_{1/2}$, $\hbar\omega_M$, $\hbar\omega_L$, S_M, and S_L being parameters, and the fitting results were shown by the green curves in Figures 5b and 6b. The optimized parameters for the fittings were summarized in Table 2, together with those for $[\mathbf{Ru(phen)_3}]^{2+}$ for comparison.

$$I(\tilde{\nu}) = \sum_{v_M=0}^{\infty}\sum_{v_L=0}^{\infty}\left(\frac{E_0 - v_M\hbar\omega_M - v_L\hbar\omega_L}{E_0}\right)^4 \times \left(\frac{S_M{}^{v_M}}{v_M!}\right) \times \left(\frac{S_L{}^{v_L}}{v_L!}\right) \times \exp\left[-4 \times \ln 2\left(\frac{\tilde{\nu} - E_0 + v_M\hbar\omega_M + v_L\hbar\omega_M}{\Delta\tilde{\nu}_{1/2}}\right)^2\right] \quad (1)$$

It has been known that the MLCT-type emission spectrum of a polypyridyl Ru(II) complex is best characterized by the ring breathing vibrations of the pyridine-type ligand and the stretching vibrations between the Ru(II) ion and ligating N atom(s) in the ligand, which are reflected on $\hbar\omega_M$ and $\hbar\omega_L$, respectively.[11a,12] In the present experiments, the $\hbar\omega_M$ and $\hbar\omega_L$ values of $[\mathbf{Ru(phen)_3}]^{2+}$ were evaluated to be 1420 and 410 cm^{-1}, respectively, and these values were very close to those reported for polypyridyl Ru(II) complexes: $\hbar\omega_M$ = 1300−1450 and $\hbar\omega_L \approx$ 400 cm^{-1}.[11a,12] The emission spectral band shapes of the $\tau^{em}(s)$ and $\tau^{em}(l)$ components observed for the complexes were very similar to that of $[\mathbf{Ru(phen)_3}]^{2+}$, and the $\hbar\omega_M$ and $\hbar\omega_L$ values were evaluated to be 1330−1380 and 380−430 cm^{-1}, respectively, for $[\mathbf{RuBE}]^{2+}$ and 1350−1400 and 400−430 cm^{-1}, respectively, for $[\mathbf{RuDE}]^{2+}$, which agreed very well with the values for the MLCT emission from polypyridyl Ru(II) complexes. Therefore, we conclude that the emission spectra of the $\tau^{em}(s)$ and $\tau^{em}(l)$ components observed for both complexes are those of an MLCT-type in nature, and this agrees very well with the results by the TD-DFT calculations.

Excited-State Origin of Dual Emissions. The dual emissions from the complex below 220 K might be explained by the inhomogeneity in the PC glass matrix medium; typically, polycrystalline states of the complex at 77 K emit emission different from that in the homogeneous environments. However, since $[\mathbf{Ru(phen)_3}]^{2+}$ under analogous conditions to those observed for $[\mathbf{RuBE}]^{2+}$ or $[\mathbf{RuDE}]^{2+}$ shows single emission below 220 K, we conclude such a possibility will be denied. Another explanation will be the emissions from the excited-state rotational isomers of the complexes. Below 220 K, rotation of the (dimesityl)borylduryl or duryl group around the ethynyl group in $[\mathbf{RuBE}]^{2+}$ or $[\mathbf{RuDE}]^{2+}$, respectively, is frozen, and each isomer may emit emission independently (i.e., dual emission), while fast rotational motions of the groups above 220 K will give rise to single emission from the complexes. However, we suppose that such a model will not explain the large differences in the $\tau^{em}(s)$ (13−14 μs) and $\tau^{em}(l)$ values (~27 μs) below 220 K as well as the almost T-independent $\tau^{em}(s)$ values of the complexes in T = 77−320 K. Furthermore, our theoretical single-point calculations for the rotational isomer of $[\mathbf{RuDE}]^{2+}$, in which duryl group is rotated by 90° from the optimized geometry, did not agree with such rotational isomer model. The HOMO−LUMO energy gap of the rotational isomer (4.41 eV) was much larger than that of the optimized geometry (3.27 eV). While the calculations were carried out for the singlet states of the complexes, the excited triplet state of the rotational isomer is also expected to be much higher energy than that of the optimized planar geometry. Therefore, we must seek another possible origin for the dual emissions from the complexes.

The lowest-energy absorption predicted for $[\mathbf{RuBE}]^{2+}$ or $[\mathbf{RuDE}]^{2+}$ is the degenerated HOMO−1/HOMO → LUMO/LUMO+3 transitions, and the HOMO → LUMO and HOMO−1 → LUMO/LUMO+3 transitions are best characterized by the MLCT transitions with large and small LC characters, respectively, as described before: see also Figure 2. We suppose that the lowest-energy excited singlet state (S_1) produced by such absorption transition in $[\mathbf{RuBE}]^{2+}$ or $[\mathbf{RuDE}]^{2+}$ splits in energy and subsequent intersystem crossing produces the excited triplet states (T_1 and T_2) separated in energy by 270−290 cm^{-1} as estimated by time-resolved emission spectroscopy (Figures 5 and 6). Although we have not succeeded in calculating singlet ground state−T_1/T_2 absorption transitions, we suppose that the lowest-energy (T_1) and second excited triplet states (T_2) of the complexes will be the MLCT states with relatively large (T_1(MLCT/LC)) and small LC characters (T_2(MLCT)), respectively, and these

DOI: 10.1021/ic502843x
Inorg. Chem. 2015, 54, 3245−3252

excited triplet states below 220 K show emission independently as schematically shown in Figure 9.

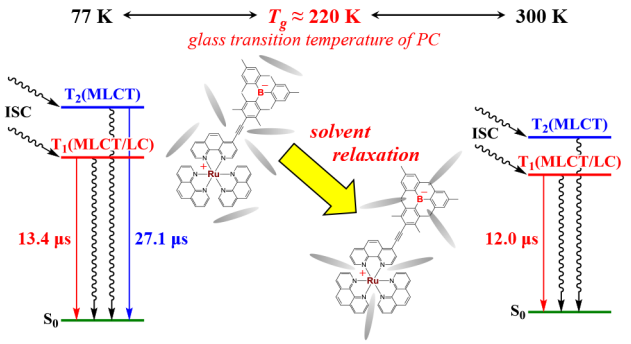

Figure 9. Energy diagram of the excited triplet states of $[\mathbf{RuBE}]^{2+}$.

It is worth pointing out that the fluid-to-glass transition temperature (T_g) in PC is ~220 K. The lower-energy T_1 ($\tau^{em}(s)$) emissions from $[\mathbf{RuBE}]^{2+}$ and $[\mathbf{RuDE}]^{2+}$ are observed irrespective of T studied (77−320 K), while the higher-energy T_2 ($\tau^{em}(l)$) emissions appear only below $T_g \approx 220$ K, and thus, the fluid-to-glass transition in PC should relate strongly to appearance/disappearance of the T_2 ($\tau^{em}(l)$) emission. Below T_g in PC, since solvent molecules are frozen and nonradiative decay through solvent reorganization/solute−solvent interactions is impeded, the T_2(MLCT) emission can be observed. In practice, such fluid-to-glass medium effects on the photophysical properties of transition metal complexes have been hitherto sometimes reported.[10,13] On the other hand, since the T_2(MLCT) state above ~220 K is highly solvated, this will facilitate fast nonradiative decay to the ground state. The T_1(MLCT/LC) state possessing a relatively large LC character will not suffice strong solvent reorganization compared with the T_2(MLCT) state and, thus, shows emission irrespective of T (77−298 K). This will be the possible origin of the dual emissions from the complexes at low temperature.

CONCLUSIONS

The present paper demonstrated that both $[\mathbf{RuBE}]^{2+}$ and $[\mathbf{RuDE}]^{2+}$ possessed spatially-isolated excited triplet MLCT states (T_1 and T_2) in close proximity in energy (270−290 cm^{-1} as estimated at 77 K) and the two excited triplet states showed independently individual emissions below 220 K. The T_1 and T_2 states of the complexes were shown to possess the MLCT/LC and MLCT characters, respectively. The T_2 MLCT excited states of the complexes showing the longer emission lifetimes ($\tau^{em}(l) \approx 27$ μs) became nonemissive above the glass-to-fluid transition temperature in PC ($T_g \approx 220$ K) owing to strong solvation around the MLCT excited states and subsequent fast nonradiative decay to the ground states, while the T_1 MLCT/LC excited states showed emission ($\tau^{em}(s) \approx 13$ μs) irrespective of T: 77−320 K. The presence of the arylethynyl group at the 4-position of the phen ligand in $[\mathbf{RuBE}]^{2+}$ or $[\mathbf{RuDE}]^{2+}$ plays important roles in the unique photophysical properties of the complex through providing the LC characters to the lowest-energy excited triplet MLCT state. In practice, our preliminary studies have confirmed that Ru(II) complexes having 4-arylethynyl-phen ligands other than $[\mathbf{RuBE}]^{2+}$ and $[\mathbf{RuDE}]^{2+}$ also exhibit dual emissions. Further studies on the spectroscopic and photophysical properties of the polypyridyl Ru(II) and Re(I) tricarbonyl complexes having a 4-/4,7-arylethynyl-phen or 4-/4,4′-arylethynyl-bpy ligand(s) are in progress in our research group, and the results will be reported in separate publications.

AUTHOR INFORMATION

Corresponding Authors

*E-mail: sakueri@nagasaki-u.ac.jp. (E.S.)
*E-mail: kitamura@sci.hokudai.ac.jp. (N.K.)

Present Address

⊥Division of Chemistry and Materials Science, Graduate School of Engineering, Nagasaki University, Bunkyo-machi, Nagasaki 852−8521, Japan

Notes

The authors declare no competing financial interest.

ACKNOWLEDGMENTS

N.K. acknowledges a grant-in-aid for Scientific Research from the Ministry of Education, Culture, Sports, Science and Technology (MEXT) of the Japanese Government for the support of the research (Nos. 25107504 (Grant-in-Aid for Scientific Research on Innovative Areas), 25620035 (Grant-in-Aid for Exploratory Research), and 26248022 (Grant-in-Aid for Scientific Research (A)).

REFERENCES

(1) Sakuda, E.; Ando, Y.; Ito, A.; Kitamura, N. *Inorg. Chem.* **2011**, *50*, 1603.

(2) (a) Van Houten, J.; Watts, R. J. *J. Am. Chem. Soc.* **1976**, *98*, 4853. (b) Van Houten, J.; Watts, R. J. *Inorg. Chem.* **1978**, *17*, 3381. (c) Durham, B.; Caspar, J. V.; Nagle, J. K.; Meyer, T. J. *J. Am. Chem. Soc.* **1982**, *104*, 4803. (d) Allen, G. H.; White, R. P.; Rillema, D. P.; Meyer, T. J. *J. Am. Chem. Soc.* **1984**, *106*, 2613. (e) Henderson, L. J., Jr.; Cherry, W. R. *J. Photochem.* **1985**, *28*, 143. (f) Wacholtz, W. F.; Auerbach, R. A.; Schmehl, R. H. *Inorg. Chem.* **1986**, *25*, 227. (g) Barrigelletti, F.; Juris, A.; Balzani, V.; Belser, P.; von Zelewsky, A. *J. Phys. Chem.* **1987**, *91*, 1095. (h) Juris, A.; Balzani, V.; Barrigelletti, F.; Campagna, S.; Belser, P.; von Zelewsky, A. *Coord. Chem. Rev.* **1988**, *84*, 85. (i) Kawanishi, Y.; Kitamura, N.; Tazuke, S. *Inorg. Chem.* **1989**, *28*, 2968. (j) Rillema, D. P.; Blanton, C. B.; Shaver, R. J.; Jackman, D. C.; Boldaji, M.; Bundy, S.; Worl, L. A.; Meyer, T. J. *Inorg. Chem.* **1992**, *31*, 1600. (k) Treadway, J. A.; Loeb, B.; Lopez, R.; Anderson, P. A.; Keene, F. R.; Meyer, T. J. *Inorg. Chem.* **1996**, *35*, 2242. (l) Zheng, G. Y.; Rillema, D. P. *Inorg. Chem.* **1996**, *35*, 7118. (m) Hammarström, L.; Barigelletti, F.; Flamigni, L.; Indelli, M. T.; Armaroli, N.; Calogero, G.; Guardigli, M.; Sour, A.; Collin, J.-P.; Sauvage, J.-P. *J. Phys. Chem. A* **1997**, *101*, 9061. (n) Wang, Y.; Peres, W.; Zheng, G. Y.; Rillema, D. P. *Inorg. Chem.* **1998**, *37*, 2051. (o) Yam, V. W.-W.; Lo, K. K.-W. *Coord. Chem. Rev.* **1999**, *184*, 157−240. (p) Wu, F.; Riesgo, E.; Paualora, A.; Kipp, R. A.; Schmehl, R. H.; Thummel, R. P. *Inorg. Chem.* **1999**, *38*, 5620. (q) Thompson, D. W.; Fleming, C. N.; Myron, B. D.; Meyer, T. J. *J. Phys. Chem. B* **2007**, *111*, 6930. (r) Abrahamsson, M.; becker, H.-C.; Hammarström, L.; Bonnefous, C.; Chamchoumis, C.; Thummel, R. P. *Inorg. Chem.* **2007**, *46*, 10354. (s) Lever, A. B. P. *Coord. Chem. Rev.* **2010**, *254*, 1397−1405. (t) Baggaley, E.; Weinstein, J. A.; Williams, J. A. G. *Coord. Chem. Rev.* **2012**, *256*, 1762−1785. (u) Lo, K. K.-W.; Choi, A. W.-T.; Law, W. H.-T. *Dalton Trans.* **2012**, *41*, 6021−6047. (v) Camilo, M. R.; Cardoso, C. R.; Carlos, R. M.; Lever, A. B. P. *Inorg. Chem.* **2014**, *53*, 3694−3708.

(3) (a) Sakuda, E.; Funahashi, A.; Kitamura, N. *Inorg. Chem.* **2006**, *45*, 10670. (b) Kitamura, N.; Sakuda, E.; Ando, Y. *Chem. Lett.* **2009**, *38*, 938. (c) Ito, A.; Hirokawa, T.; Sakuda, E.; Kitamura, N. *Chem. Lett.* **2011**, *40*, 34. (d) Ito, A.; Kang, Y.; Saito, S.; Sakuda, E.; Kitamura, N. *Inorg. Chem.* **2012**, *51*, 7722.

(4) (a) Wallace, L.; Rillema, D. P. *Inorg. Chem.* **1993**, *32*, 3836. (b) Wallace, L.; Woods, C.; Rillema, D. P. *Inorg. Chem.* **1995**, *34*, 2875.

DOI: 10.1021/ic502843x
Inorg. Chem. 2015, 54, 3245−3252

(c) Wallace, L.; Jackman, D. C.; Rillema, D. P.; Merkert, J. *Inorg. Chem.* **1995**, *34*, 5210.
(5) (a) Glazer, E. C.; Nagde, D.; Tor, Y. *J. Am. Chem. Soc.* **2005**, *127*, 4190. (b) Glazer, E. C.; Magde, D.; Tor, Y. *J. Am. Chem. Soc.* **2007**, *129*, 8544. (c) Magde, D.; Magde, M. D. Jr.; Glazer, E. C. *Coord. Chem. Rev.* In press, DOI: 10.1016/j.ccr.2015.01.003.
(6) Elangovan, A.; Yang, S.-W.; Lin, J.-H.; Kao, K.-M.; Ho, T.-I. *Org. Biomol. Chem.* **2004**, *2*, 1597.
(7) Perrin, D. D.; Armarego, W. L. F.; Perrin, D. R. *Purification of Laboratory Chemicals,* 2nd ed.; Pargamon Press: New York, 1980.
(8) Frisch, M. J.; Trucks, G. W.; Schlegel, H. B.; Scuseria, G. E.; Robb, M. A.; Cheeseman, J. R.; Scalmani, G.; Barone, V.; Mennucci, B.; Petersson, G. A.; Nakatsuji, H.; Caricato, M.; Li, X.; Hratchian, H. P.; Izmaylov, A. F.; Bloino, J.; Zheng, G.; Sonnenberg, J. L.; Hada, M.; Ehara, M.; Toyota, K.; Fukuda, R.; Hasegawa, J.; Ishida, M.; Nakajima, T.; Honda, Y.; Kitao, O.; Nakai, H.; Vreven, T.; Montgomery, J. A., Jr.; Peralta, J. E.; Ogliaro, F.; Bearpark, M.; Heyd, J. J.; Brothers, E.; Kudin, K. N.; Staroverov, V. N.; Kobayashi, R.; Normand, J.; Raghavachari, K.; Rendell, A.; Burant, J. C.; Iyengar, S. S.; Tomasi, J.; Cossi, M.; Rega, N.; Millam, N. J.; Klene, M.; Knox, J. E.; Cross, J. B.; Bakken, V.; Adamo, C.; Jaramillo, J.; Gomperts, R.; Stratmann, R. E.; Yazyev, O.; Austin, A. J.; Cammi, R.; Pomelli, C.; Ochterski, J. W.; Martin, R. L.; Morokuma, K.; Zakrzewski, V. G.; Voth, G. A.; Salvador, P.; Dannenberg, J. J.; Dapprich, S.; Daniels, A. D.; Farkas, Ö.; Foresman, J. B.; Ortiz, J. V.; Cioslowski, J.; Fox, D. J. *Gaussian 09,* Revision A.1; Gaussian, Inc.: Wallingford, CT, 2009.
(9) Dennington, R.; Keith, T.; Millam, J. *GaussView,* Version 5; Semichem Inc: Shawnee Mission, KS, 2009.
(10) (a) Kitamura, N.; Kim, H.-B.; Kawanishi, Y.; Obata, R.; Tazuke, S. *J. Phys. Chem.* **1986**, *90*, 1488. (b) Kim, H.-B.; Kitamura, N.; Tazuke, S. *Chem. Phys. Lett.* **1988**, *143*, 77. (c) Kim, H.-B.; Kitamura, N.; Tazuke, S. *J. Phys. Chem.* **1990**, *94*, 1414. (d) Kim, H.-B.; Kitamura, N.; Tazuke, S. *J. Phys. Chem.* **1990**, *94*, 7401.
(11) (a) Ito, A.; Meyer, T. J. *Phys. Chem. Chem. Phys.* **2012**, *14*, 13731. (b) Kent, C. A.; Liu, D.; Ito, A.; Zhang, T.; Brennaman, M. K.; Meyer, T. J.; Lin, W. *J. Mater. Chem. A* **2013**, *1*, 14982. (c) Thompson, D. W.; Ito, A.; Meyer, T. J. *Pure Appl. Chem.* **2013**, *85*, 1257. (d) Zanoni, K. P. S.; Kariyazaki, B. K.; Ito, A.; Brennaman, M. K.; Meyer, T. J.; Murakami Iha, N. Y. *Inorg. Chem.* **2014**, *53*, 4089.
(12) Caspar, J. V.; Westmoreland, T. D.; Allen, G. H.; Bradley, P. G.; Meyer, T. J.; Woodruff, W. H. *J. Am. Chem. Soc.* **1984**, *106*, 3492.
(13) (a) Knight, T. E.; Goldstein, A. P.; Brennaman, M. K.; Cardolaccia, T.; Pandya, A.; DeSimone, J. M.; Meyer, T. J. *J. Phys. Chem. B* **2011**, *115*, 64. (b) Ito, A.; Knight, T. E.; Stewart, D. J.; Brennaman, M. K.; Meyer, T. J. *J. Phys. Chem. A* **2014**, *118*, 10326.

DOI: 10.1021/ic502843x
Inorg. Chem. 2015, 54, 3245−3252